Welding in the World (2024) 68:427–440
https://doi.org/10.1007/s40194-023-01663-8

RESEARCH PAPER

Behaviour of aluminium/steel hybrid RSW joints under high cycle fatigue loading

Ákos Meilinger[1] · Mariann Fodorné Cserépi[1] · János Lukács[1]

Received: 13 September 2023 / Accepted: 8 December 2023 / Published online: 18 December 2023

Abstract

The lightweight construction of automotive car bodies is the more important to reduce the fuel consumption and costs. High-strength steels and aluminium alloys are suitable for achieving these aims. Recent car bodies contain both materials, therefore necessary to make reliable joints between them. The resistance spot welding (RSW) can be used for joining of car bodies and it is applicable for aluminium/steel hybrid joints, too. High cycle fatigue (HCF) test results can be rarely found in the literature while HCF loading basically determines the lifetime of hybrid joints. 5754-H22, 6082-T6, and DP600 base materials were used for similar and hybrid RSW joints and HCF tests were performed. Number of cycles to failure values, failure modes, furthermore brittle intermetallic compound (IMC) layers were studied and analysed. In both aluminium/steel hybrid joints, the HCF test results showed better endurance limit like concerning aluminium/aluminium similar joints, but worse than steel/steel joints. For 5754-H22 alloy the endurance limit values are 648 N, 939 N, and 1285.5 N, for similar aluminium, hybrid, and similar steel joints, respectively. For 6082-T6 alloy these values are 513 N, 625.5 N, and 1285.5 N, respectively. In case of similar joints only base material fracture happens, but hybrid joint specimens show different failure modes. Base material fracture and shearing after partial base material fracture were typical failure modes in case of 5754-H22/DP600 and 6082-T6/DP600 hybrid joints, respectively. The full and partial plugging as a failure modes appeared for hybrid joints, too. The IMC layer characteristics showed opposite results in cases of hybrid joints, both the layer thicknesses of the shared and plugged joints and the thickness differences between the inner and outer parts of the joints were different.

Keywords Hybrid joint · Aluminium/steel joining · Resistance spot welding (RSW) · High cycle fatigue (HCF)

1 Introduction

Nowadays, the aluminium/steel joining occurs typically in automotive industry in case of car bodies, for example energy absorption elements are frequently made from aluminium/steel structure. The structural elements should be joined and these joints can be made by mechanical joining methods like self-piercing riveting [1–3] or clinching [4–6]; furthermore, the welding [7–9] can be used for this aim, too. In case of self-piercing riveting the tensile-shear or cross-tension static tests show appropriate joint strength quality [1, 10], but the rivet used makes the procedure more expensive. Clinching process is not expensive, since no additives are needed, but the joint strength is characteristically weaker. In some cases, the mechanical joining methods are supplemented by adhesive bonding [11], which is a relatively expensive technology; the welding can be more cost effective. In case of welding, basically the resistance spot welding (RSW) and the ultrasonic welding (UW) can be applied for hybrid spot joining [12–14]. In recent years special process variants appeared to improve the joint properties, like resistance element welding (REW) [15], metallic bump assisted RSW (MBaRSW) [16], (high power) ultrasonic welding ((HP)USW) [17], ultrasonic, and resistance spot welding combination [18]. Micro-RSW (MRSW) [19] and vaporizing foil actuator welding (WFAW) [20] were also investigated

Recommended for publication by Commission XIII—Fatigue of Welded Components and Structures

✉ János Lukács
janos.lukacs@uni-miskolc.hu

Ákos Meilinger
akos.meilinger@uni-miskolc.hu

Mariann Fodorné Cserépi
mariann.cserepi@uni-miskolc.hu

[1] Institute of Material Science and Technology, University of Miskolc, 3515 Miskolc-Egyetemváros, Hungary

as prospective solutions for aluminium/steel joining. The special joining methods require additional materials and/or process steps, or the process cycle is longer in comparison with the original RSW. Table 1 summarises different joining processes used for aluminium/steel joining and their main characteristics.

Some investigation [8, 10] highlighted that the RSW is just rarely used for aluminium/steel sheet joining because the presence of brittle intermetallic compound (IMC) and necessary to remove the oxide layer from the aluminium part before welding. Furthermore, the welding task is challenging because of the absolutely different material properties (melting point, thermal conductivity, electrical resistance, strength). The joint strength can be improved with removed oxide layer, but the oxide removing during manufacturing cannot be efficient and cheap enough [36]. The forming IMC layer is very brittle, and the joint properties are influenced by IMC thickness and containing phase type. A thin IMC layer (thinner than 10 μm) has no significant effect on the strength and ductility of the joints, but the thick IMC layer can be harmful applying laser welding [37]. In case of RSW, different values of the optimal IMC layer thickness were concluded in the joint interface. Zhang et al. recommended maximum 5 μm [38]; Chen et al. reported 3 μm [29]; and Miyamoto determined it as 2 μm [39]. For this aim, it is generally necessary to keep the process temperature and duration as low and short as possible, because the formation of the IMC layers requires atomic diffusion. Several studies were performed to identify the significant IMC phases and their effects on the joint properties. Sundman et al. [40] reported that the possible IMCs at room temperature are Al_2Fe, Al_5Fe_2, and Al_3Fe_4. Kouadri-David et al. [41] analysed the IMC regions and found that the critical region of an IMC is the aluminium side, which contains more Al but there is a significant Fe fraction, too. This is because the solubility of Al in Fe is greater than the solubility of Fe in

Table 1 Joining technologies for aluminium/steel spot joining

Joining process	Aluminium material	Steel material	Coating or additional material and form	Source
RSW	A5052	A366/A366M-97	Commercial steel cover plate in aluminium side	[21]
	A5052	SUS304	Commercial steel cover plate in aluminium side	
	A5052	DP600	Pure Zn interlayer	[22]
	AW5754-H22	DP500	DP500 uncoated	[23]
	5182-O	SAE 1008	1050 clad SAE 1006 transition material	[24]
	6008-T6	H220YD	H220YD galvanised	[25]
	6008-T6	H220YD	H220YD galvanised; 4047 AlSi12 interlayer	[26]
	AA6022-T4	Interstitial free steel (IFS)	IFS hot-dipped galvanised	[27, 28]
	AA6022-T4	Low carbon steel (LCS)	LCS hot-dipped galvanised	[29]
	AA6022-T4	Mild steel (MS)	MS hot-dipped galvanised	[30]
	X626	Low carbon steel (LCS)	LCS uncoated	[31]
	AA6022	Low carbon steel (LCS)	LCS uncoated	
	AA6022	HSLA steel	HSLA steel uncoated	
	A6061	AISI-SAE 1005	Pure Cu insert	[32]
	A6061	AISI-SAE 1005	Pure Zn insert	
	6063-T6	16Mn	16Mn uncoated	[33]
	Al6K32	SGARC440	SGARC uncoated	[34]
	Al6K32	SGARC440	SGARC Zn coated	
MBaRSW	AA6061-T6	DP590	DP590 uncoated	[16]
MRSW	AA1100	SS301	Low carbon steel (LCS) interlayer	[19]
REW	AW5754-H22	DP500	Q235 steel rivet in aluminium side	[23]
	AA6061-T6	HS1300T	HS1300T Al–Si coated; SWRCH16A solid rivet in aluminium side	[15]
(HP)USW	6061-T6	AISI 304	AISI 304 uncoated	[35]
	6061-T6	ASTM A36	ASTM A36 uncoated	
	Al-6011	DC04	DC04 uncoated	[17]
	Al-6011	DX53-ZF	DX53-ZF hard galvannealed Zn coating	
	Al-6011	DX56-Z	DX56-Z soft hot-dipped Zn coating	
USW + RSW	A6061-T6	AISI 1008	A6061-T6 insert	[18]
VFAW	5A06	SS321	3003 interlayer	[20]

Al, and the Al-rich IMC phases are brittle, while the Fe-rich phases are relatively ductile. Therefore, the joint properties can be improved if the formations of Al rich brittle IMCs are minimised. Zhang et al. [38] found that the main IMC phases are Fe_2Al_5 on the steel side and $FeAl_3$ or Fe_4Al_{13} on the aluminium side, where the previous one is thicker than the last one. The morphology and thickness of the IMC layer depend on the process parameters and on the distance from the centre of the joint; the thickness is generally higher at the joint centre and lower on the boundary [30]. Fe_2Al_5 was identified as the dominant phase in the IMC layer formed at the joint interface. The Fe_2Al_5 grew; it evolved from randomly oriented fine grains to coarse grains with preferred direction, perpendicular to the aluminium/steel interface. Numerical simulation was performed; it was found that the majority of Fe_2Al_5 growth occurred when the temperature between the sheets was over 900 ℃. The growth of Fe_2Al_5 reduces the joint strength and can cause interfacial fracture. Cracks within Fe_2Al_5 mainly consisted of primary cracks propagating through the interface and secondary cracks approaching the steel side, while the primary cracks became the dominant ones with increased IMC thickness [42].

According to literature and our previous investigations [36, 43], under quasi-static loading conditions the strength properties of aluminium/steel RSW joints can be comparable with aluminium/aluminium joints. Table 2 shows tensile-shear test results performed on different aluminium/steel combinations compared with the tensile-shear strengths of aluminium/aluminium similar joint.

The table shows that there is no significant difference between similar aluminium and hybrid aluminium/steel joints based on the results of tensile-shear strength. However, the typical loading condition of a car body is the cyclic loading, and the aluminium/steel hybrid joints can show different behaviours under high cycle fatigue. In case of quasi-static loading, the thickness of IMC layer has influence on the mechanical behaviour of the joint; consequently under cyclic loading condition, the effect of IMC can be important, too. The IMC properties were investigated widely and connected to the quasi-static-type mechanical test results and their failure modes. The behaviour of aluminium/steel hybrid joints under cyclic loading is rarely investigated [27, 28, 31, 48]. The results have shown that the behaviour of aluminium/steel RSW joints under cyclic loading condition was better than aluminium/aluminium joints [27, 28], applying special electrode for the welding process. At the same time, most of the previous investigations were carried out using different aluminium and steel plate thicknesses and those were not covered the fatigue limit range of the S–N curves in none of the cases. The latter is also important because steels can be characterised by a definite fatigue limit, whereas aluminium alloys cannot. Furthermore, the comparisons were completed for a minority of the investigations; they were not covered the full steel/steel, aluminium/steel, and aluminium/aluminium variations. Therefore, the basic aims of our research (in medium term) are to compare aluminium/steel joining technologies and to optimise the technologies based on different criteria. The direct objective of the research and this article (in short term) is to give more and quantitative information about the aluminium/steel RSW joint properties under cyclic loading condition (high cycle fatigue).

Table 2 Results of tensile-shear tests in case of aluminium/steel and aluminium/aluminium RSW joints

Material grades	Thicknesses (mm)	Tensile-shear force (kN)	Remark	Source
5754-H22/DP800	1 + 1	2.44	Average value	[36]
5754-H22/5754-H22	1 + 1	2.04	Average value	[43]
AA5754/AA5754	1 + 1	2.60	Average value	[44]
AA5754/AA5754	2 + 3	5.5	Average value	
6082-T6/DP800	1 + 1	2.51	Average value	[36]
6082-T6/6082-T6	1 + 1	2.44	Average value	[43]
6082-T6/6082-T6	1 + 1	3.23	Best value	[45]
6082-T6/6082-T6	1 + 1	2.75	Best value	[46]
Al 6K32/SGARC440	1.6 + 1.4	5.20	Best value	[34]
Al 6K32/SGARC440	1 + 1	3.47	Best value	
6061-T6/DP780	1.5 + 1.5	2.38	Best value	[47]
AA6022/AA6022	1.2 + 1.2	3.50	From diagram	[48]
AA6022/HSLA	1.2 + 2.0	5.30	From diagram	
AA6061/Q235	2.0 + 1.0	5.86	Best value	[49]
X6262/LCS	0.8 + 0.9	2.90	Average value	[50]
AA6022/LCS	1.2 + 1.2	4.25	Average value	

Table 3 Chemical compositions of the applied aluminium alloys, based on quality certificates, weight %

Material grade	Cu	Fe	Mn	Cr	Mg	Ti	Si	Zn	Al
5754-H22	0.055	0.294	0.358	0.009	2.796	0.016	0.193	0.034	rest
6082-T6	0.09	0.46	0.46	0.02	0.7	0.03	0.9	0.08	rest

Table 4 Chemical composition of the applied DP steel, based on quality certificate, weight %

Material grade	C	Si	Mn	P	S	Nb	V	B	Fe
DP600	0.098	0.2	0.81	0.015	0.002	0.014	0.01	0.0002	rest

Table 5 Basic mechanical properties of base materials, based on quality certificates

Material grade	R_m (MPa)	$R_{p0.2}$ (MPa)	A_{50} (%)
5754-H22	220	137	22
6082-T6	348	303	15
DP600	669	448	18.7

2 Materials and technologies

DP600 steel was chosen as the steel part; it is frequently used in the automotive industry and has relatively low strength between dual-phase (DP) steels. DP steels contain hard martensite islands embedded in a ferrite matrix with a dispersed distribution. The steel side was combined with 5754-H22 aluminium alloy (strain hardened) as the first combination and with 6082-T6 aluminium alloy (heat treated) as the second combination. The 5754-H22 aluminium sheet is one of the commonly used material qualities, mainly due to its good formability and associated appropriate strength properties. Its main alloying element is Mg, its strength increased by forming, and then softened to a quarter of hardness. The weldability of this alloy is good among the aluminium alloys. The 6082-T6 base material is one of the most widely used heat-treatable aluminium alloys; it has lower formability and higher strength. It contains mainly Mg and Si alloying elements which are causing ageing. This alloy is more sensitive for welding, softening in the heat-affected zone, and hot cracking can easily happen because welding. For the experiments both similar (steel/steel, aluminium alloy/aluminium alloy) and hybrid (steel/aluminium alloy) joints were produced. Each base material had 1 mm thickness for better comparability.

Tables 3 and 4 show the chemical compositions; furthermore, Table 5 summarises the most important mechanical properties (tensile strength (R_m), yield strength ($R_{p0.2}$), and elongation (A_{50})) of the base materials according to quality certificates.

A TECNA 8007-type welding machine (AC, 50 Hz) with TE 550-type control system was used for welding; the welding force was ensured by a pneumatic cylinder. The weld control mode was constant current mode. The electrode material was CuCrZr; according to RWMA, it is in the class 2. The welding electrodes were used with a 5-mm spherical pin diameter. The radius of the spherical pin was $R = 50$ mm, according to the recommendation of the literature [51, 52]. The same geometry was used for the upper and lower electrodes (see Fig. 1).

The used parameter combinations are previously optimised based on tensile-shear test results, Table 6 summarises the chosen parameters and resulted weld nugget/joint diameters. These parameters gave the thinnest IMC layers, lower heat input causes lack of joining, and higher heat input results thicker IMC. In case of 5754-H22/DP600 joints, 10% higher current was needed than 6082-T6/DP600 joints.

3 Testing circumstances

The high cycle fatigue (HCF) tests were carried out according to the guidelines of the relevant standard [53]. The geometry and the dimensions of the test specimens for all base material combinations with 1 mm sheet thickness can be seen in Fig. 2. The specimen parts were cut from 1000 mm × 2000 mm dimension sheets into 100 × 30 mm dimensions strips. The investigated RSW joint located at the centre of the 30 mm overlapped area.

HCF tests were carried out by MTS 322.41 electro-hydraulic universal material testing equipment and MTS FlexTest 40 controller. Sinusoidal loading wave form was used, the applied load ratio (F_{min}/F_{max}) was $R = 0.1$ with $f = 30$ Hz frequency. During the HCF tests in all cases, several load levels were applied at room temperature and in laboratory air. Considering that the tests were evaluated according to [54, 55], the load levels were chosen as described in that document. Displacement limit detector was not used, so the cycles counted until complete failure. Figure 3 shows the test specimen gripping in the test system, using both a schematic and a real image.

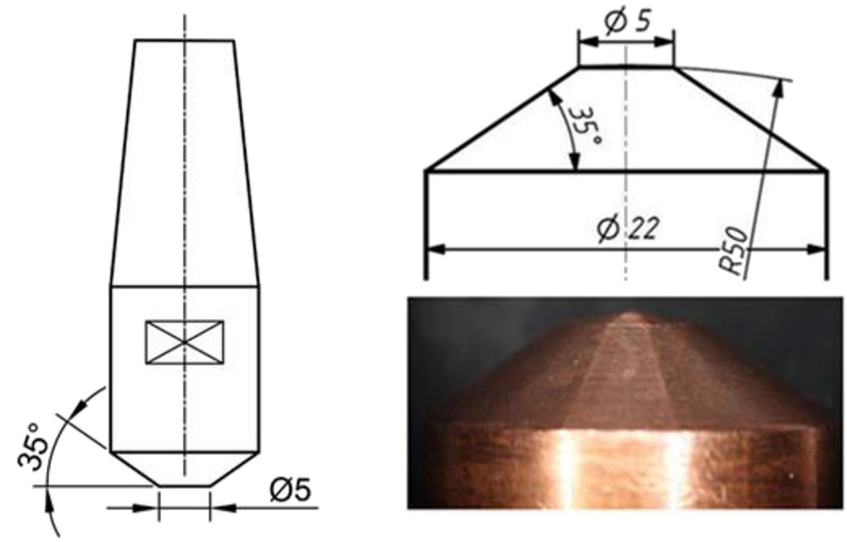

Fig. 1 The geometry of the upper and lower welding electrodes

Table 6 Parameter combinations for RSW and resulted weld nugget/joint diameters

Material combination	Welding current (kA)	Welding time (ms)	Welding force (kN)	Weld nugget/joint diameter (mm)
5754-H22/DP600	16.5	220	2.5	6.8–7.2
6082-T6/DP600	15	220	2.5	6.7–7.1
5754-H22/5754-H22	24	100	2.5	5.8–6.1
6082-T6/6082-T6	23	100	2.5	5.8–6.0
DP600/DP600	8.5	320	4	7.3–7.5

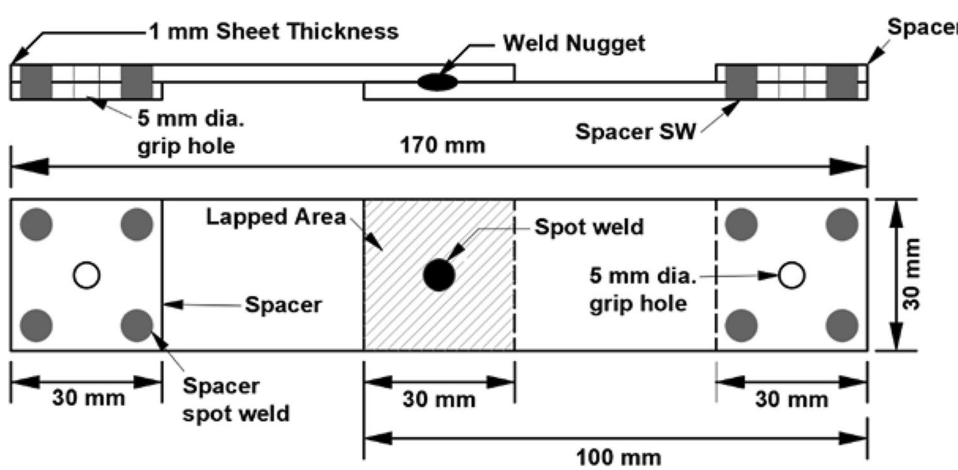

Fig. 2 HCF test sample geometry and dimensions

4 Results and discussions

The number of cycles to failure values was recorded after HCF tests. The results of fatigue tests were plotted by load range (ΔL) to a number of cycles to failure (N) using a logarithmic scale for the number of cycles in ΔL-N curve. Figure 4 shows the ΔL-N curves of DP600 and 5754-H22 similar and hybrid joint combinations, where the arrows indicate surviving specimens. The straight lines were determined using the least squares method (lifetime section) and calculating the mean values (endurance limit); therefore, they belong to the 50% probability. The figure clearly shows that the DP600 similar joints have the best result as it is predicted; the endurance limit was 1282.5 N. The 5754-H22 similar joints result the worst value; the

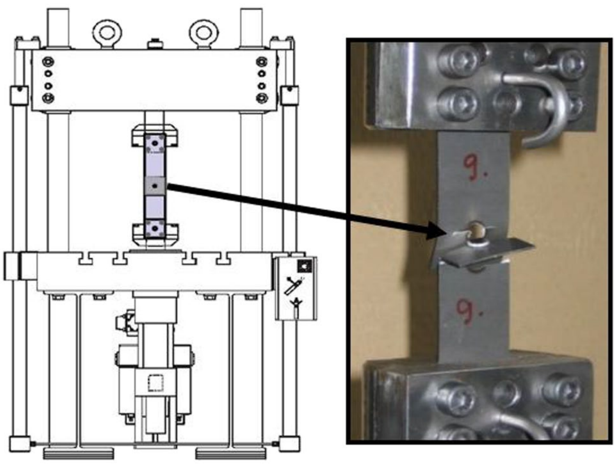

Fig. 3 HCF test specimen gripping in the test system and a specimen after the fatigue test

endurance limit was 648 N, which is nearly the half of the steel. The 5754-H22/DP600 hybrid joints show significantly better result than the aluminium alloy, with 939 N endurance limit value.

Figure 5 shows the result of HCF tests in case of DP600 and 6082-T6 similar and hybrid joints. The nature and trend of the results are the same as those shown in Fig. 4 for DP600 and 5754-H22 materials. In this case the endurance limit of hybrid joints is 625.5 N, which is significantly lower than DP600 steel joints (1282.5 N); furthermore, the 6082-T6 similar joints gave the worst result, the endurance limit was 513 N. The difference between the steel joints and the hybrid joints was larger than for the 5754-H22 alloy; in other words, the difference between the hybrid joint and the aluminium joint was smaller than for the 5754-H22 alloy.

Figure 6 shows all HCF test results compared with literature data [27]. The high cycle fatigue resistance of 5754-H22/DP600 hybrid joints are significantly better than 6082-T6/DP600 hybrid joints and competitive with the result from the literature. According to literature data [27], the endurance limit is approximately same in case of 6022-T4/IF steel hybrid and 6022-T4/6022-T4 similar joints, and shows slight difference between our result (6082-T6/DP600, 5754-H22/5754-H22). It should be noted that in [27], article fatigue limit values were not specified and wider (38 mm instead of 30 mm) and thicker (1.2 mm aluminium alloy and 3 mm IF steel instead of 1 mm) specimens were used.

Table 7 summarises the characteristics of the ΔL-N curves belonging to 50% probability, using

$$\Delta L = A * ln(N) + B \tag{1}$$

Basquin-type [56] equation. The data in the literature are consistent with our test results, and it can be concluded that the 5754-H22/DP600 joints show a better fatigue limit than the 5754-H22/DP500 joints [23]. It should be noted that the 5754-H22/DP500 joints were made with REW process (Q235 steel rivet in aluminium side) and thicker steel plate (1.5 mm instead of 1 mm).

Failure modes after HCF showed different and not typical types in some cases. Tables 8, 9, 10, and 11 summarise these types in the failure mode column. In some cases, the base material fracture was combined with shearing. In these cases, it can be assumed that the crack started in the upper side of the spot from the heat-affected zone,

Fig. 4 ΔL-N curves for DP600/DP600, 5754-H22/DP600, and 5754-H22/5754-H22 joints

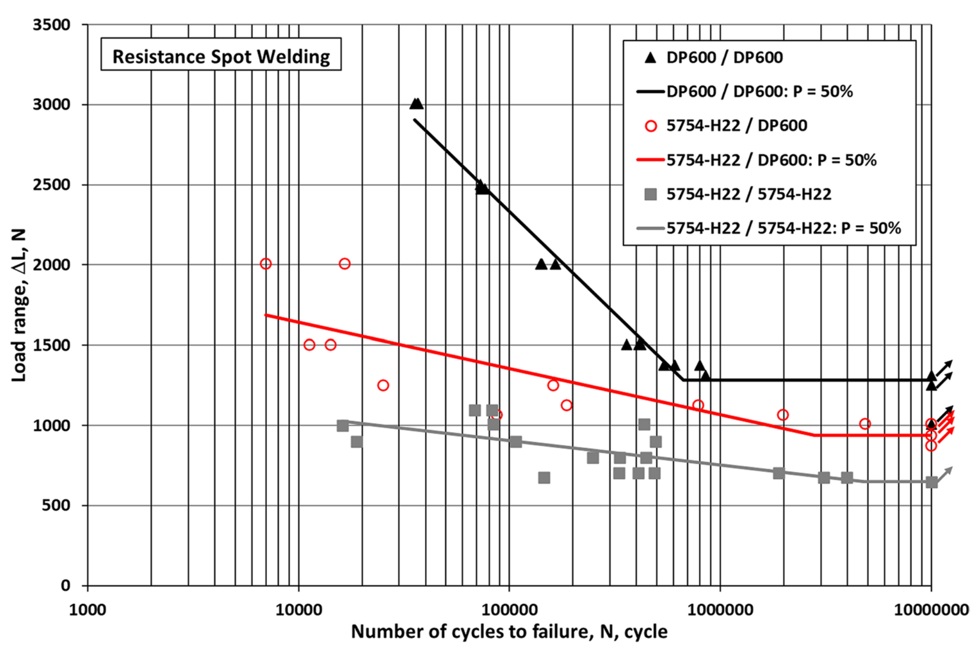

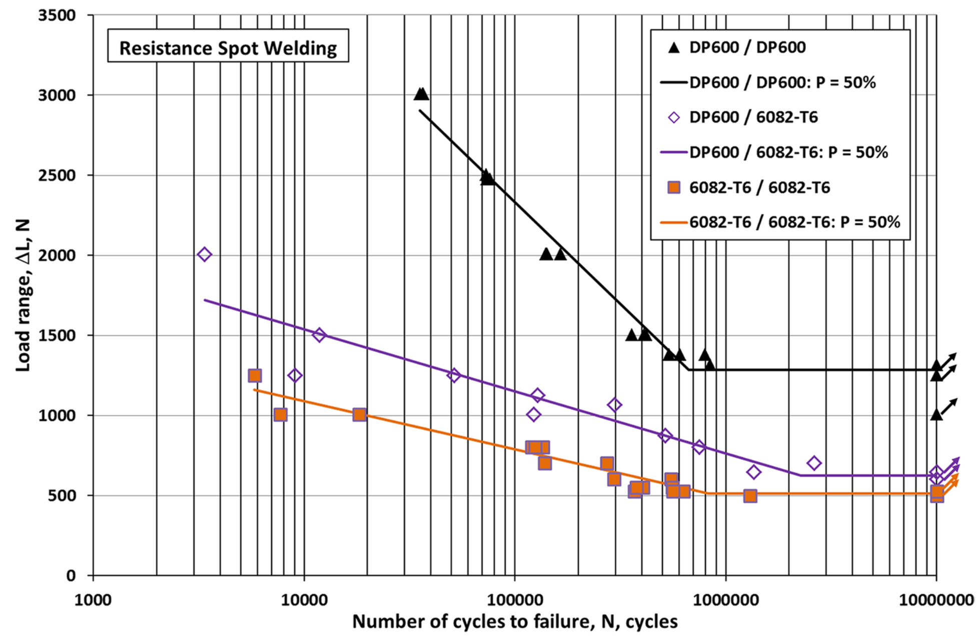

Fig. 5 ΔL-N curves for DP600/DP600, 6082-T6/DP600, and 6082-T6/6082-T6 joints

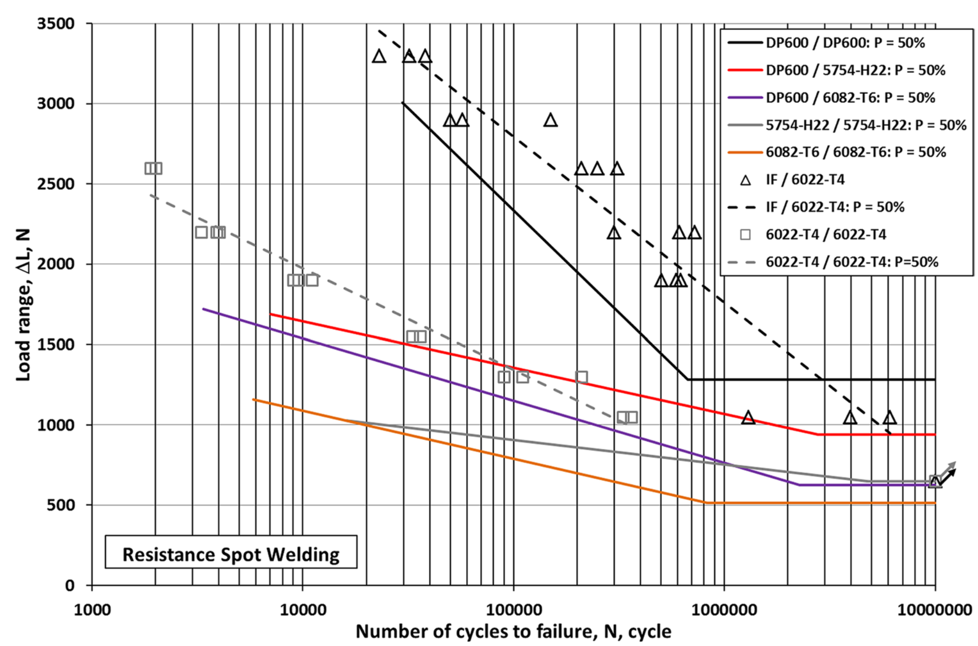

Fig. 6 All high cycle fatigue results compared with literature data [27]

then growing to the base material, but it cannot propagate fully because shearing happens in the joint line. The other failure mode in case of hybrid joint is the clear shearing, which is not typical in case of steel/steel or aluminium/aluminium joints. The 5754-H22/5754-H22, 6082-T6/6082-T6, and DP600/DP600 joints showed the same failure mode, base material fracture. Figure 7 shows the macrostructure of failure modes in all cases.

Tables 8, 9, and 10 show the numerical data of the results and failure modes for all specimens in case of DP600/DP600, 5754-H22/5754-H22, and 6082-T6/6082-T6 joints, respectively.

Tables 11 and 12 show the numerical results of HCF tests in case of hybrid joints including the failure modes.

In hybrid joint cases, the failure modes were different. Partial or full plugging happens in case of low number of cycles, however, mostly base material fracture with or without shearing, and shearing happens in higher number of cycles.

Table 7 Characteristics of the ΔL-N curves belonging to 50% probability

Material combination	A	B	Correlation coefficient	ΔL_{el} (N)	Source
DP600/DP600	– 552.9	8699	0.985	1285.5	This study
5754-H22/DP600	– 125.1	2795	0.770	939	This study
5754-H22/DP500	– 19.26	2167	N/A	882	[23]
6082-T6/DP600	– 167.9	3083	0.929	625.5	This study
IF/6022-T4	– 449.2	7966	0.952	N/A	[27]
6022-T4/6022-T4	– 274.2	4498	0.981	N/A	
5754-H22/5754-H22	– 66.4	1668	0.668	648	This study
6082-T6/6082-T6	– 133.0	2313	0.963	513	This study

After HCF tests selected cross-sections of resistance spot welded joints were examined, focusing on different failure modes. Based on the observed failure modes (see Table 11 and 12), cross-sections of sheared/base material fracture and plugged fracture types were selected. In case of sheared/base material fracture type, the IMC layer was identified on the steel part, and cannot be found on the aluminium part, in line with previous experiences [41]. Thus, in this case, the IMC layer thickness can be measured and it assumed as the full IMC thickness. In case of plugged and base material fracture types, the IMC thicknesses were easily measured between the two base materials. Figures 8 and 9 show the result of the measurements on 5754-H22/DP600 and 6082-T6/ DP600 joints, respectively. In the background cross-section of plugged type can be seen.

In case of 5754-H22/DP600 plugged failure mode, the IMC layer thickness is much lower in the whole joint line than the sheared one; the IMC thicknesses are between 0.85 and 1.32 µm. The thickness of the sheared type is between 1.1 and 2.26 µm. It means that the IMC thickness of plugged type is bigger and more equal than in case of the sheared type. The 5754-H22/DP600 plugged cross-section shows that the outer part of the joint was sheared, and the bigger inner part is plugged. By the IMC layer thickness measurement, it can be clearly identified that the IMC thickness in the inner part is bigger like in the outer part. The IMC thickness on the plugged part is more than 1.1 µm, just a small increasing happens (1.32 µm) in the centre of the joint. In this specimen the thinner IMC shows shearing.

In case of 6082-T6/DP600, the plugged joint has significantly bigger IMC layer thicknesses in the whole joint line, and the sheared one shows thinner IMC. The IMC thickness of plugged type was between 1.2 and 2.92 µm, and the thickness of IMC in case of sheared one was between 0.55 and 1.89 µm.

Table 8 Load range, number of cycles to failure values, and failure modes in case of DP600/DP600 similar joint specimens

Specimen ID	Load range (N)	Number of cycles to failure (cycle)	Failure mode
33	3006	35,520	Base material fracture
34	2007	140,746	Base material fracture
35	1008	10,138,542	Survived (not broken)
36	1503	359,251	Base material fracture
37	1251	10,000,000	Survived (not broken)
38	1503	410,346	Base material fracture
39	2007	141,607	Base material fracture
40	3006	36,823	Base material fracture
41	2007	142,182	Base material fracture
42	1377	607,580	Base material fracture
43	1377	797,583	Base material fracture
44	1314	10,000,000	Survived (not broken)
49	2475	76,375	Base material fracture
50	2475	73,477	Base material fracture
51	3006	36,678	Base material fracture
52	1377	540,601	Base material fracture
53	1503	419,171	Base material fracture
54	2007	164,834	Base material fracture
55	2502	73,009	Base material fracture
56	1314	847,412	Base material fracture

The IMC thicknesses show big differences through the joint line in both cases. The 6082-T6/DP600 plugged cross-section shows a little bit smaller plug diameter, and the outer part is also sheared here. The IMC thickness of the sheared part is less than 1.5 µm. In the plugged part, the IMC thickness is increasing from 1.5 to 2.92 µm. In this specimen the thinner IMC shows shearing, too, like in case of 5754/DP600 plugged case, but the IMC thickness is bigger.

Table 9 Load range, number of cycles to failure values, and failure modes in case of 5754-H22/5754-H22 similar joint specimens

Specimen ID	Load range (N)	Number of cycles to failure (cycle)	Failure mode
A01	1008	83,956	Base material fracture
A02	900	106,775	Base material fracture
A03	801	332,734	Base material fracture
A04	702	484,822	Base material fracture
A05	1098	82,422	Base material fracture
A06	999	16,113	Base material fracture
A07	900	18,831	Base material fracture
A08	801	444,664	Base material fracture
A09	702	330,452	Base material fracture
A10	648	10,000,000	Survived (not broken)
A11	1098	68,304	Base material fracture
A12	1008	433,582	Base material fracture
A13	900	491,930	Base material fracture
A14	702	1,891,283	Base material fracture
A15	675	146,000	Base material fracture
A16	801	248,263	Base material fracture
A17	702	408,593	Base material fracture
A18	675	3,968,226	Base material fracture
A19	675	3,078,847	Base material fracture
A01	1008	83,956	Base material fracture
A02	900	106,775	Base material fracture

Table 10 Load range, number of cycles to failure values, and failure modes in case of 6082-T6/6082-T6 similar joint specimens

Specimen ID	Load range (N)	Number of cycles to failure (cycle)	Failure mode
AA02	1251	5823	Base material fracture
AA03	1008	18,213	Base material fracture
AA04	801	135,908	Base material fracture
AA05	702	138,919	Base material fracture
AA06	603	552,418	Base material fracture
AA07	801	120,097	Base material fracture
AA08	702	274,024	Base material fracture
AA09	603	294,715	Base material fracture
AA10	549	403,812	Base material fracture
AA11	549	559,077	Base material fracture
AA12	1008	7689	Base material fracture
AA13	526.5	630,165	Base material fracture
AA14	526.5	368,298	Base material fracture
AA15	499.5	1,301,891	Base material fracture
AA16	499.5	10,000,000	Survived (not broken)
AA17	526.5	10,000,000	Survived (not broken)
AA18	549	378,107	Base material fracture
AA19	526.5	562,136	Base material fracture
AA20	801	124,559	Base material fracture

5 Conclusions

Based on the executed and evaluated investigations and their results, the following conclusions can be drawn.

- The applied joining technologies gave comparable HCF test results on similar and hybrid RSW joints of DP600, 5754-H22, and 6082-T6 base materials.
- The endurance limit of 5754-H22/DP600 hybrid joints was higher (939 N) than 5754-H22/5754-H22 similar joints (648 N), but lower than DP600/DP600 similar joints (1285.5 N). The endurance limit of 6082-T6/DP600 hybrid joints was higher (625.5 N) than 6082-T6/6082-T6 similar joints (513 N), but lower than DP600/DP600 similar joints (1285.5 N). The tendency was similar to that for 5754-H22 aluminium alloy, but

Table 11 Load range, number of cycles to failure values, and failure modes in case of 6082-T6/DP600 hybrid joint specimens

Specimen ID	Load range (N)	Number of cycles to failure (cycle)	Failure mode
CsM015	1008	122,672	Base material partial fracture + shearing
CsM016	873	518,730	Base material partial fracture + shearing
CsM017	801	749,165	Base material partial fracture + shearing
CsM018	702	2,625,109	Base material partial fracture + shearing
CsM019	2007	3379	Partial plugging
CsM020	1251	9031	Base material partial fracture + shearing
CsM021	1125	127,917	Base material partial fracture + shearing
CsM022	648	1,361,264	Base material fracture
CsM024	603	10,000,000	Survived (not broken)
CsM025	648	10,000,000	Survived (not broken)
CsM026	1503	11,810	Base material partial fracture + shearing
CsM027	1251	51,537	Full plugging
CsM028	1066.5	298,120	Base material fracture

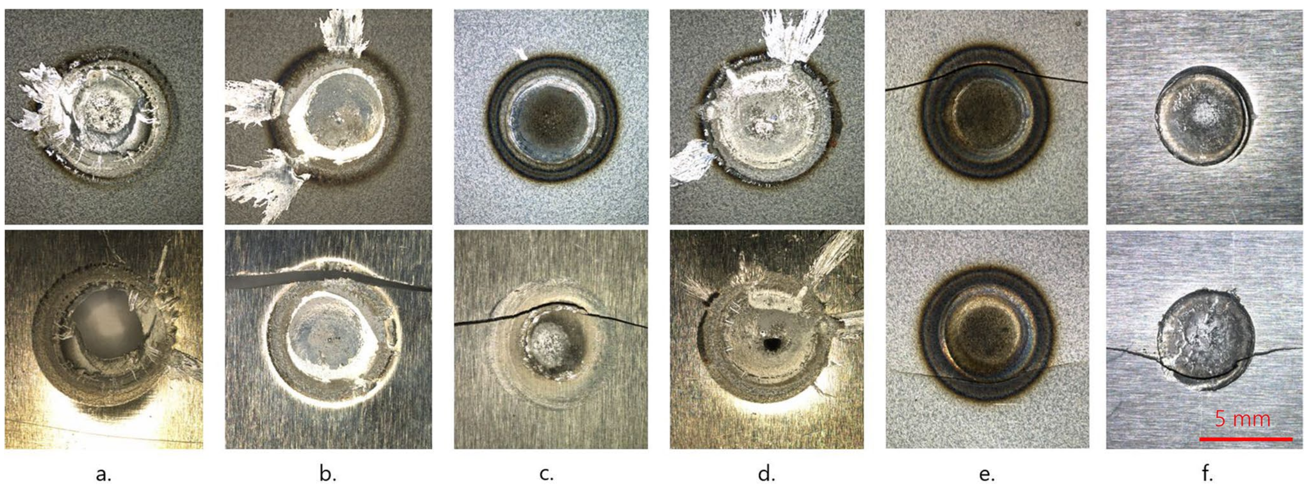

Fig. 7 Failure modes of RSW joints: **a** full plugging (aluminium/steel), **b** base material partial fracture + shearing (aluminium/steel), **c** base material fracture (aluminium/steel), **d** shearing (aluminium/steel), **e** base material fracture (steel/steel), and **f** base metal fracture (aluminium/aluminium)

the difference between aluminium and steel similar joints was larger (772.5 N vs. 637.5 N), while the difference between aluminium and hybrid joints was smaller (112.5 N vs. 291 N). No relevant, directly comparable HCF test data were found in the literature.

- Only base material fracture was experienced for all similar welded joints; however, different failure modes were observed for hybrid joints. Base material fracture and shearing after partial base material fracture were the typical failure modes in case of 5754-H22/DP600 and 6082-T6/DP600 hybrid joints, respectively. Furthermore, in some cases, full and partial plugging as a failure modes were appeared for hybrid joints.
- IMC layer thicknesses were measured in case of plugging, as well as of partial base material fracture and shearing failure modes. Thicker IMC layer was measured in case of sheared 5754-H22/DP600 joint than the plugged one, and the IMC thickness was bigger in joint centre than the outer part. In addition, smaller differences were measured between the inner and outer parts of plugged joint. Opposite results can be detected for 6082-T6/DP600 joint. The IMC layer thickness was thinner in

Table 12 Load range, number of cycles to failure values, and failure modes in case of 5754-H22/DP600 hybrid joint specimens

Specimen ID	Load range (N)	Number of cycles to failure (cycle)	Failure mode
CsM001	1251	161,569	Base material fracture
CsM002	1008	4,852,014	Shearing
CsM003	1125	785,622	Base material fracture
CsM004	873	10,000,000	Survived (not broken)
CsM04_No2	2007	7010	Full plugging
CsM005	936	10,000,000	Survived (not broken)
CsM006	1008	10,000,000	Survived (not broken)
CsM008	2007	16,562	Full plugging
CsM009	1503	14,163	Base material fracture
CsM010	1066.5	1,972,535	Base material partial fracture + shearing
CsM011	1125	186,960	Base material fracture
CsM012	1251	25,127	Base material fracture
CsM013	1503	11,257	Base material fracture
CsM014	1066.5	86,859	Base material fracture

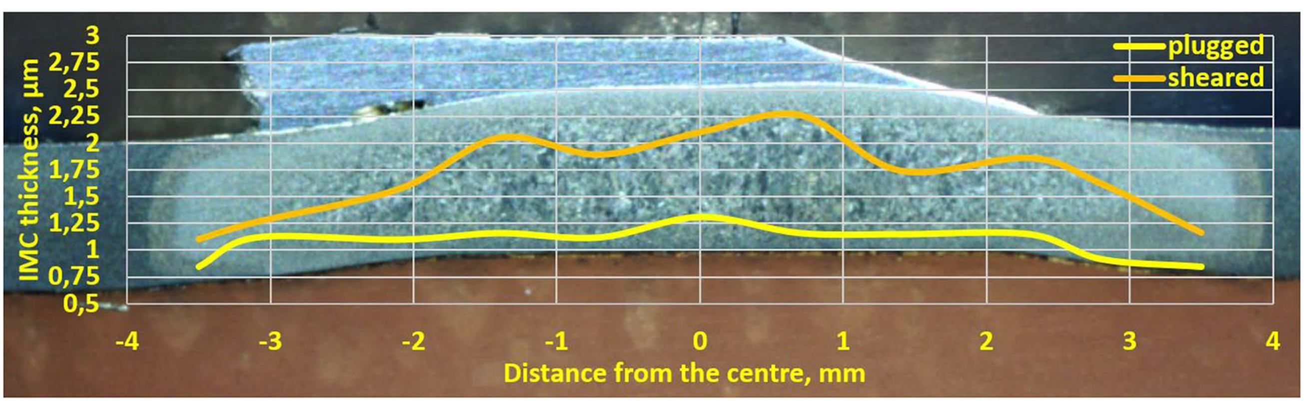

Fig. 8 IMC thicknesses in the joint line in case of 5754-H22/DP600 plugged and sheared specimens

case of sheared one, and thicker in case of plugged one. Furthermore, there are significant differences in IMC thicknesses between the inner and outer parts of the joint.

- In case of plugged failure mode, it is clearly visible that the plug diameter is smaller than the IMC layer diameter. The 5754-H22/DP600-plugged specimens show well-definable IMC thickness where the plug exists (1.1 µm); however, for 6082-T6/DP600, this could not be determined perfectly.
- In order to compare hybrid joints, further investigations are needed:

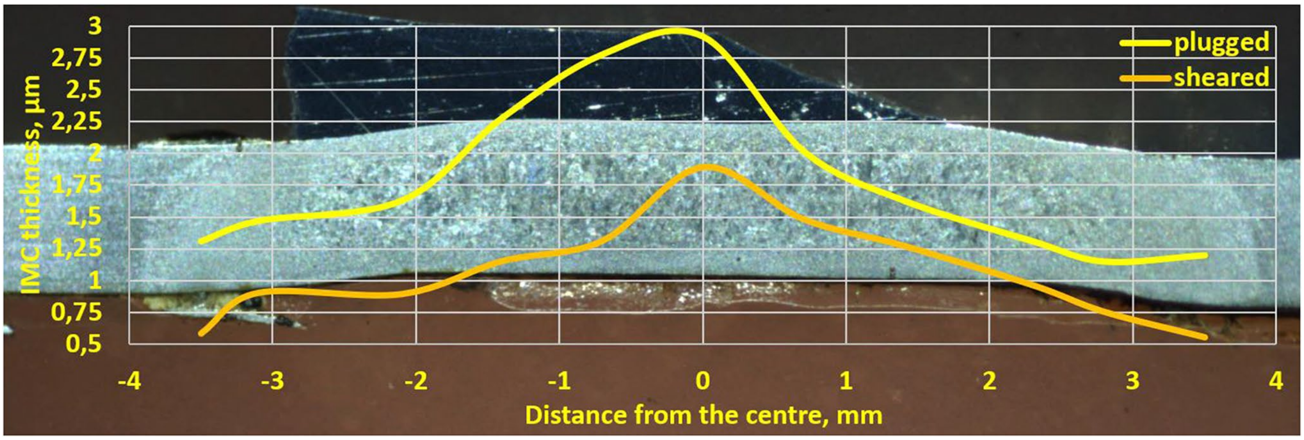

Fig. 9 IMC thicknesses in the joint line in case of 6082-T6/DP600 plugged and sheared specimens

- joints made with other technologies (e.g. clinching) should be performed;
- HCF tests should be executed and evaluated;
- fatigue crack growth (FCG) test should be prepared, executed, and evaluated;
- both different technologies and cyclic behaviours should be compared and optimal application areas should be specified.

Acknowledgements This research was supported by the European Union and the Hungarian State, co-financed by the European Structural and Investment Funds in the framework of the GINOP-2.3.4-15-2016-00004 project, aimed to promote the cooperation between the higher education and the industry.

Funding Open access funding provided by University of Miskolc.

Declarations

Conflict of Interest The authors declare no competing interests.

References

1. Karathanasopoulos N, Mohr D (2022) Strength and failure of self-piercing riveted aluminum and steel sheet joints: multi-axial experiments and modeling. J Adv Join Process 5(100107):1–9. https://doi.org/10.1016/j.jajp.2022.100107
2. Zhou ZJ, Huang ZC, Jiang YQ, Tang NL (2022) Joining properties of SPFC440/AA5052 multi-material self-piercing riveting joints. Materials 15(2962):1–17. https://doi.org/10.3390/ma15092962
3. Zhang YC, Huang ZC, Jiang YQ, Jia YL (2023) Mechanical properties of B1500HS/AA5052 joints by self-piercing riveting. Metals 13(328):1–19. https://doi.org/10.3390/met13020328
4. Lee CJ, Kim JY, Lee SK, Ko DC, Kim BM (2010) Parametric study on mechanical clinching process for joining aluminum alloy and high-strength steel sheets. J Mech Sci Technol 24:123–126. https://doi.org/10.1007/s12206-009-1118-5
5. Jiang T, Zhong-Xia Liu ZX, Wang PC (2015) Quality inspection of clinched joints of steel and aluminum. Int J Adv Manuf Technol 76:1393–1402. https://doi.org/10.1007/s00170-014-6362-x
6. Sz J, Tisza M, Felhős D, Kovács PZ (2019) Experimental and numerical study of dissimilar sheet metal clinching. AIP Conf Proc 2113:050021. https://doi.org/10.1063/1.5112585
7. Pouranvari M (2017) Critical assessment 27: dissimilar resistance spot welding of aluminium/steel: challenges and opportunities. Mater Sci Technol 33(15):1705–1712. https://doi.org/10.1080/02670836.2017.1334310
8. Gullino A, Matteis P, D'Aiuto F (2019) Review of aluminum-to-steel welding technologies for car-body applications. Metals 9:315. https://doi.org/10.3390/met9030315
9. Lu Y, Zhang K, Tran J, Mayton E, Kimchi M, Zhang W (2019) Optimizing ultrasonic plus resistance spot welding for dissimilar metal joining. Weld J 98:273–282. https://doi.org/10.29391/2019.98.024
10. Sakiyama T, Gen Murayama G, Yasuaki, Naito Y, Kenji Saita K, Miyazaki Y, Oikawa H, Nose T (2013) Dissimilar metal joining technologies for steel sheet and aluminum alloy sheet in auto body. Nippon Steel Technical Report No. 103:91–97. https://www.nipponsteel.com/en/tech/report/nsc/pdf/103-14.pdf. Accessed 14 Sept 2023
11. Guzanová A, Brezinová J, Varga J, Džupon M, Vojtko M, Janoško E, Vináš J, Draganovská D, Hašul J (2023) Experimental study of steel–aluminum joints made by RSW with insert element and adhesive bonding. Materials 16:864. https://doi.org/10.3390/ma16020864
12. Haddadi F (2016) Microstructure reaction control of dissimilar automotive aluminium to galvanized steel sheets ultrasonic spot welding. Mater Sci Eng A 678:72–84. https://doi.org/10.1016/j.msea.2016.09.093

13. Zhao D, Ren D, Zhao K, Pan S, Guo X (2017) Effect of welding parameters on tensile strength of ultrasonic spot welded joints of aluminum to steel—by experimentation and artificial neural network. J Manuf Process 30:63–74. https://doi.org/10.1016/j.jmapro.2017.08.009
14 Patel VK, Bhole SD, Chen DL (2014) Ultrasonic spot welding of aluminum to high-strength low-alloy steel: microstructure, tensile and fatigue properties. Metall and Mater Trans A 45:2055–2066. https://doi.org/10.1007/s11661-013-2123-y
15. Sizhe N, Ming L, Yunwu M, Yongbing L (2021) Study on the microstructure and mechanical performance for integrated resistance element welded aluminum alloy/press hardened steel joints. Mater Sci Eng A 800:140329. https://doi.org/10.1016/j.msea.2020.140329
16. Guotao Z, Hang Z, Xianghe X, Guohua Q, Yongbing L, Zhongqin L (2019) Metallic bump assisted resistance spot welding (MBaRSW) of AA6061-T6 and Bare DP590: part II-joining mechanism and joint property. J Manuf Process 44:19–27. https://doi.org/10.1016/j.jmapro.2019.05.041
17. Farid H, Fadi AF (2015) Microstructural and mechanical performance of aluminium to steel high power ultrasonic spot welding. J Mater Process Technol 225:262–274. https://doi.org/10.1016/j.jmatprotec.2015.06.019
18. Ying L, Ellis M, Hyeyun S, Menachem K, Wei Z (2019) Dissimilar metal joining of aluminum to steel by ultrasonic plus resistance spot welding - microstructure and mechanical properties. Mater Des 165:107585. https://doi.org/10.1016/j.matdes.2019.107585
19. Baskoro AS, Muzakki H, Kiswanto G, Winarto W (2018) Effect of interlayer in dissimilar metal of stainless steel SS 301 and aluminum alloy AA 1100 using micro resistance spot welding. AIP Conf Proc 1983:040014. https://doi.org/10.1063/1.5046271
20. Shan S, Shujun C, Yu M, Jun X, Anupam V, Glenn D (2019) Joining aluminium alloy 5A06 to stainless steel 321 by vaporizing foil actuators welding with an interlayer. Metals 9:43. https://doi.org/10.3390/met9010043
21. Ranfeng Q, Chihiro I, Shinobu S (2009) Interfacial microstructure and strength of steel/aluminum alloy joints welded by resistance spot welding with cover plate. J Mater Process Technol 209:4186–4193. https://doi.org/10.1016/j.jmatprotec.2008.11.003
22. Jianbin C, Xinjian Y, Zhan H, Ting L, Kanglong W, Lm Ci (2017) Improvement of resistance-spot-welded joints for DP 600 steel and A5052 aluminum alloy with Zn slice interlayer. J Manuf Process 30:396–405. https://doi.org/10.1016/j.jmapro.2017.10.009
23. Aleksija Đ, Dragan M, Zijah B, Damjan K, Miodrag M, Biljana M, Vladislav K (2022) Microstructure and fatigue properties of resistance element welded joints of DP500 steel and AW 5754 H22 aluminum alloy. Crystals 12:258. https://doi.org/10.3390/cryst12020258
24. Sun X, Stephens EV, Khaleel MA, Shao H, Kimchi M (2004) Resistance spot welding of aluminum alloy to steel with transition material from process to performance part I: experimental study. Weld J 83(6):188-S–195-S. http://files.aws.org/wj/supplement/wj0604-188.pdf. Accessed 14 Sept 2023
25. Weihua Z, Daqian S, Lijun H, Yongqiang L (2015) Optimised design of electrode morphology for novel dissimilar resistance spot welding of aluminium alloy and galvanised high strength steel. Mater Des 85:461–470. https://doi.org/10.1016/j.matdes.2015.07.025
26. Weihua Z, Daqian S, Lijun H, Dongyang L (2013) Interfacial microstructure and mechanical property of resistance spot welded joint of high strength steel and aluminium alloy with 4047 AlSi12 interlayer. Mater Des 57:186–194. https://doi.org/10.1016/j.matdes.2013.12.045
27. Jidong K, Harish MR, David RS, Blair EC (2017) Tensile and fatigue behaviour of AA6022-T4 to IF steel resistance spot weld. Procedia Struct Integr 5:1425–1432. https://doi.org/10.1016/j.prostr.2017.07.207
28. Harish MR, Jidong K, Liting S, David RS, Blair EC (2018) Effect of specimen configuration on fatigue properties of dissimilar aluminum to steel resistance spot welds. Int J Fatigue 116:13–21. https://doi.org/10.1016/j.ijfatigue.2018.06.009
29. Nannan C, Hui-Ping W, Blair EC, David RSS, Min W (2017) Fracture mechanisms of Al/steel resistance spot welds in lap shear test. J Mater Process Technol 243:347–354. https://doi.org/10.1016/j.jmatprotec.2016.12.015
30. Zixuan W, Hui-Ping W, Nannan C, Min W, Blair EC (2017) Characterization of intermetallic compound at the interfaces of Al-steel resistance spot welds. J Mater Process Technol 242:12–23. https://doi.org/10.1016/j.jmatprotec.2016.11.017
31. Liting S, Jidong K, Mark G, Xu C, Amberlee SH, Blair EC (2020) Fatigue life assessment of Al-steel resistance spot welds using the maximum principal strain approach considering material inhomogeneity. Int J Fatigue 140:105851. https://doi.org/10.1016/j.ijfatigue.2020.105851
32. Al-Filfily AA, Al-Adili AS, Sar MH (2020) Strength of resistance spot welding of aluminum alloy AA6061 to carbon steel using different filler materials. IOP Conf Ser: Mater Sci Eng 881:012067. https://doi.org/10.1088/1757-899X/881/1/012067
33. Daqian S, Yueying Z, Yanjun L, Xiaoyan G, Hongmei L (2016) Microstructures and mechanical properties of resistance spot welded joints of 16Mn steel and 6063–T6 aluminum alloy with different electrodes. Mater Des 109:596–608. https://doi.org/10.1016/j.matdes.2016.07.076
34. Seungmin S, Dae-Jin P, Jiyoung Y, Sehun R (2019) Resistance spot welding of aluminum alloy and carbon steel with spooling process tapes. Metals 9:410. https://doi.org/10.3390/met9040410
35. Mirza FA, Macwan A, Bhole SD, Chen DL, Chen XG (2016) Effect of welding energy on microstructure and strength of ultrasonic spot welded dissimilar joints of aluminum to steel sheets. Mater SciEng A 668:73–85. https://doi.org/10.1016/j.msea.2016.05.040
36 Sahm A, Gáspár M, Meilinger Á (2022) Properties of hybrid aluminium-steel joints made by resistance spot welding. Defect Diffus Forum. 416:131–138. https://doi.org/10.1016/j.jmatprotec.2008.11.003
37. Meco S, Pardal G, Ganguly S, Williams S, McPherson N (2015) Application of laser in seam welding of dissimilar steel to aluminium joints for thick structural components. Opt Lasers Eng 67:22–30. https://doi.org/10.1016/j.optlaseng.2014.10.006
38. Zhang W, Sun D, Han L, Gao W, Qiu X (2011) Characterization of intermetallic compounds in dissimilar material resistance spot welded joint of high strength steel and aluminum alloy. ISIJ Int 51:1870–1877. https://doi.org/10.2355/isijinternational.51.1870
39. Miyamoto K, Nakagawa S, Sugi C, Sakurai H, Hirose A (2009) Dissimilar joining of aluminum alloy and steel by resistance spot welding. SAE Int J Mater Manuf 2:58–67. https://www.jstor.org/stable/26282734
40 Sundman B, Ohnuma I, Dupin N, Kattner UR, Fries SG (2009) An assessment of the entire Al–Fe system including DO3 ordering. Acta Mater 57:2896–2908. https://doi.org/10.1016/j.actamat.2009.02.046
41. Kouadri-David A, PSM Team (2014) Study of metallurgic and mechanical properties of laser welded heterogeneous joints between DP600 galvanised steel and aluminium 6082. Mater Des 54:184–195. https://doi.org/10.1016/j.matdes.2013.07.093
42. Nannan C, Min W, Hui-Ping W, Zixuan W, Blair EC (2018) Microstructural and mechanical evolution of Al/steel interface with Fe_2Al_5 growth in resistance spot welding of aluminum to

steel. J Manuf Process 34(2018):424–434. https://doi.org/10.1016/j.jmapro.2018.06.024
43 Gáspár M, Tervo H, Kaijalainen Dobosy Á, Török I (2018) The effect of solution annealing and ageing during the RSW of 6082 aluminium alloy. VAE 2018: Veh Automot Eng 2:694–708. https://doi.org/10.1007/978-3-319-75677-6_59
44. Hana L, Thorntona M, Boomerb D, Shergold M (2011) A correlation study of mechanical strength of resistance spot welding of AA5754 aluminium alloy. J Mater Process Technol 211:513–521. https://doi.org/10.1016/j.jmatprotec.2010.11.004
45. Pereira AM, Ferreira JM, Loureiro A, Costa JDM, Bártolo PJ (2010) Effect of process parameters on the strength of resistance spot welds in 6082–T6 aluminium alloy. Mater Des 31:2454–2463. https://doi.org/10.1016/j.matdes.2009.11.052
46. Lakhani AM (2018) Experimental investigation on resistance spot welding of aluminium alloy 6082-T651 using interlayer of SS304. International J Mech Eng Technol 9(7):313-324. https://iaeme.com/MasterAdmin/Journal_uploads/IJMET/VOLUME_9_ISSUE_7/IJMET_09_07_036.pdf. Accessed 14 Sept 2023
47. Kang Z, Baokai R, Wenxiao Y (2023) Optimized designing of generalized electrodes for aluminum/steel resistance spot welding process based on numerical calculation. J Manuf Process 99:563–580. https://doi.org/10.1016/j.jmapro.2023.05.079
48. Liting S, Jidong K, Gesinga M, Chen X, Haselhuhnc AS, Blair EC (2020) Effect of notch root angle on fatigue behavior of aluminum to steel resistance spot welds. Int J Fatigue 141:105866. https://doi.org/10.1016/j.ijfatigue.2020.105866
49. Ranfeng Q, Li J, Hongxin S, Hua Y (2023) Characterization of resistance spot welded joints between aluminum alloy and mild steel with composite electrodes. J Mater Res Technol 24:1190–1202. https://doi.org/10.1016/j.jmrt.2023.03.069
50. Liting S, Jidong K, Chen X, Haselhuhnc AS, Siglerc DR, Blair EC (2019) Determination of fracture modes in novel aluminum-steel dissimilar resistance spot welds. Procedia Struct Integr 17:355–362. https://doi.org/10.1016/j.prostr.2019.08.047
51 Akbolatov E, Kiselev SA, Slobodyan SM (2019) Prediction and stabilization of initial resistance between electrodes for small-scale resistance spot welding. Weld World 63:443–457. https://doi.org/10.1007/s40194-018-0671-x
52. Gáspár M, Dobosy Á, Tisza M, Török I, Yangchun D, Kailun Z (2020) Improving the properties of AA7075 resistance spot-welded joints by chemical oxide removal and post weld heat treating. Weld World 64:2119–2128. https://doi.org/10.1007/s40194-020-00988-y
53. International Organization for Standardization (2003) ISO 14324: resistance spot welding — destructive tests of welds — method for the fatigue testing of spot welded joints
54. The Japan Society of Mechanical Engineers (1981) JSME S 002: standard method of statistical fatigue testing
55. Nakazawa H, Kodama S (1987) Statistical S-N testing method with 14 specimens: JSME standard method for determination of S-N curves. In: Tanaka T, Nishijima S, Ichikawa M (eds.) Statistical research on fatigue and fracture. Current Japanese materials research – Vol. 2, 1st edn. Elsevier Appl Sci Soc Mater Sci Japan, pp 59–69
56. Basquin OH (1910) The exponential law of endurance tests. Proceedings of the Thirteenth Annual Meeting (X). Atlantic City, New Jersey, June 28 – July 2, 1910. American Society for Testing and Materials, pp. 625–630